

Effect of Screening of Intermicellar Interactions on the Linear and Nonlinear Rheology of a Viscoelastic Gel

Ranjini Bandyopadhyay and A. K. Sood

Department of Physics, Indian Institute of Science, Bangalore 560 012, India

Abstract

We report our studies of the linear and nonlinear rheology of aqueous solutions of the surfactant cetyl trimethylammonium tosylate (CTAT) with varying amounts of sodium chloride (NaCl). The CTAT concentration is fixed at 42mM and the salt concentration is varied between 0mM to 120mM. On increasing the salt (NaCl) concentration, we see three distinct regimes in the zero-shear viscosity and the high frequency plateau modulus data. In regime I, the zero-shear viscosity shows a weak increase with salt concentration due to enhanced micellar growth. The decrease in the zero-shear viscosities with salt concentration in regimes II and III can be explained in terms of inter-micellar branching. The most intriguing feature of our data however, is the anomalous behavior of the high frequency plateau modulus in regime II ($0.12 \leq \frac{[NaCl]}{[CTAT]} \leq 1.42$). In this regime, the plateau modulus *increases* with an increase in NaCl concentration. This is highly counter-intuitive, since the correlation length of concentration fluctuations and hence the plateau modulus G_o are not expected to change appreciably in the semi-dilute regime. We propose to explain the changes in regime II in terms of the unbinding of the organic counterions (tosylate) from the CTA^+ surfaces on the addition of NaCl. In the nonlinear flow curves of the samples with high salt content, significant deviations from the predictions of the Giesekus model for entangled micelles are observed.

1 Introduction

The flow behavior of surfactant solutions have been studied extensively, both theoretically and experimentally [1, 2]. Viscoelastic gels, which are formed by the entanglement of cylindrical micelles under appropriate conditions of temperature and salinity and in the presence of suitable counterions, can be used as model systems for rheological research. Even though the internal structures of these materials are often very complex, the viscoelastic parameters characterizing them are found to follow very simple scaling laws, making the prediction of their physical properties possible. In this paper, we focus on the effects of screening of intermicellar interactions, achieved by adding suitable amounts of the salt NaCl to CTAT samples, on the linear and nonlinear rheology of the viscoelastic gel phase. The most interesting feature of this work is the existence of an anomalous regime of salt (NaCl) concentration where the high frequency plateau modulus G_o *increases* on the addition of salt. The maximum value of G_o occurs when $\frac{[NaCl]}{[CTAT]} \sim 1.42$, where [NaCl] and [CTAT] represent the molarities of NaCl (42 mM) and CTAT (60mM), respectively. Interestingly, even as the slope of G_o changes sign on increasing salt concentration, there is no change in the slope of the relaxation time τ_R , while the slope of the zero-shear viscosity η_o plotted *vs.* salt concentration shows a significant decrease.

Theoretical and experimental studies on the effect of electrostatics on the growth of cylindrical micelles in the semi-dilute regime show a much stronger concentration dependence of the dynamical properties in salt-free conditions than in the highly screened case. Kern *et al.* have studied the effect of an increase in the concentration of the dimeric gemini surfactant on the micellar size, in the absence of added salt [3]. On increasing surfactant concentration c beyond the overlap concentration c^* , the zero shear viscosity η_o shows a very strong increase. In addition to this, the high frequency plateau modulus G_o shows a stronger concentration dependence than in the highly screened case ($G_o \sim c^3$ for unscreened micelles, in contrast to the prediction $G_o \sim c^{\frac{9}{4}}$ for highly screened, flexible micelles) [3]. Experiments on cetyl trimethylammonium chloride (CTAC) in the presence of sodium salicylate (NaSal) show a tendency towards a mono-exponential stress relaxation process with increase in the surfactant concentration c , or a decrease in the temperature T [4]. In these experiments, the scaling relations for the zero-shear viscosity η_o and the high frequency plateau modulus G_o are given by $\eta_o \sim c^{1.1}$

and $G_o \sim c^{1.7}$, where c is surfactant (CTAC) concentration. These scaling relations are found to be different from the theoretical model of Cates [5], which predicts $\eta_o \sim c^{3.7}$ and $G_o \sim c^{2-2.3}$. These anomalies are explained in terms of the non-uniform distribution of the bound chloride and salicylate ions in the end-caps and along the lengths of the cylindrical micelles [4]. These experimental results prompted MacKintosh *et al.* [6] to analytically study the effect of electrostatics on the growth of cylindrical micelles. Considering the interaction of counterions with each other, the self-energy of the free charges and the interaction of the counterions with the surface charge density to be the main contributions to the electrostatic repulsion between micelles, Mackintosh *et al.* find that charged, unscreened micelles exhibit three regimes of micellar growth with a tendency for very rapid growth in the semi-dilute regime. Screened micelles, on the other hand, show a simple and more gradual power-law growth in the semi-dilute regimes.

1.1 Theoretical models and some experimental results

In contrast to polymer solutions, micellar systems have a molecular weight distribution (MWD) at thermal equilibrium [2]. In generalizing the theory of polymers to describe the equilibrium properties of self-assembling cylindrical micelles (also called *living polymers* or *wormlike micelles*), care has to be taken to ensure a realistic length or molecular weight distribution, which may be done within the framework of the Flory-Huggins theory [7].

1.1.1 The reptation-reaction theory

The dynamics of polymeric macromolecules is well understood in terms of the reptation model [7, 8]. Reptation dynamics implies the curvilinear diffusion of a polymer chain through an imaginary tube along its own contour. In this model, it is assumed that the stress relaxation in polymers on the application of a strain results in the deformation of the chain, so that the polymer reptates out of the chain to occupy a new tube which is in equilibrium and carries no strain [8]. For a monodisperse system, the fraction of the stress $G(t)$ remaining at time t due to the application of a strain at $t = 0$ is given by [2]

$$G(t) = \frac{8}{\pi^2} \sum_{p=\text{odd}} p^{-2} \exp\left(\frac{-tp^2}{\tau_{rep}}\right) \quad (1)$$

which implies a decay of the stress with a dominant relaxation time $\tau_{rep} \approx \frac{\bar{L}^2}{D_c}$, D_c being the diffusion coefficient of the reptating chain and \bar{L} its average length.

In the case of living polymers with an equilibrium MWD, the contribution due to the breaking and recombination of chains on a time scale τ_{break} should also be accounted for. If $\tau_{break} \gg \tau_{rep}$, the relaxation function may be written as [5]

$$G(t) \sim \exp\left[-\text{constant} * \left(\frac{t}{\tau_{rep}}\right)^{\frac{1}{4}}\right] \quad (2)$$

which indicates a non-exponential stress decay.

Experimentally, a purely exponential stress relaxation has been found in many surfactant solutions [1, 2, 3, 4] where the dynamics obey $\tau_{break} \ll \tau_{rep}$. In such cases, the relaxation spectrum shows a single-exponential behavior and the viscoelastic moduli of the material are given by the well-known Maxwell model [2, 9]

$$G'(\omega) = G_o \frac{\omega^2 \tau_R^2}{1 + \omega^2 \tau_R^2} \quad (3)$$

$$G''(\omega) = G_o \frac{\omega \tau_R}{1 + \omega^2 \tau_R^2} \quad (4)$$

where $G'(\omega)$ and $G''(\omega)$ are the elastic and viscous moduli respectively, and the complex modulus $G^*(\omega) = G'(\omega) + iG''(\omega)$. In Eqns. 3 and 4, G_o is the high frequency plateau modulus, ω is the angular frequency of the applied oscillatory stress and τ_R is a characteristic relaxation time of the sample given by $\tau_R = (\tau_{rep}\tau_{break})^{\frac{1}{2}}$. The complex viscosity $\eta^*(\omega)$ may be written in terms of $G'(\omega)$ and $G''(\omega)$ as follows

$$\eta^*(\omega) = \frac{\sqrt{G'(\omega)^2 + G''(\omega)^2}}{\omega} \quad (5)$$

For viscoelastic gels, the complex viscosity is given by [9]

$$|\eta^*(\omega)| = \frac{\eta_o}{\sqrt{1 + \omega^2 \tau_R^2}} \quad (6)$$

In the Maxwell model, the zero-shear viscosity η_o is given by

$$\eta_o = G_o \tau_R \quad (7)$$

For a distribution of relaxation times, the stress relaxation may be fitted to a stretched exponential model given by

$$G(t) \sim \exp[-constant * (\frac{t}{\tau_{rep}})^\alpha] \quad (8)$$

where the exponent α depends on the surfactant concentration, salinity and temperature, and tends to 1 when $\tau_{break} \ll \tau_{rep}$. In the frequency domain, the corresponding form is the empirical Cole Davidson model [10], where the complex relaxation $G^*(\omega)$ can be described as

$$G^*(\omega) = G_o [1 - \frac{1}{(1 + i\omega\tau_R)^\alpha}] \quad (9)$$

where G_o corresponds to $G(\omega \rightarrow \infty)$. G_o can be used to estimate ξ , the correlation length of concentration fluctuations, by using the relation $G_o \sim \frac{k_B T}{\xi^3}$ [2, 11].

1.1.2 The Giesekus model

The Giesekus model [12] can be used to predict the nonlinear flow properties of surfactant solutions. This model uses the reptation theory as the starting point and introduces a deformation-dependent mobility tensor β in order to account for the orientation effects of flow. Using a linear dependence between β and the configuration tensor C , and combining this equation with the upper-convected Maxwell equation $\beta\sigma = \tau_R \frac{\partial\sigma}{\partial t} = 2\eta\dot{\gamma}$, where σ is the shear stress, $\dot{\gamma}$ is the shear rate and τ_R is the characteristic relaxation time, Giesekus obtained the following relations between rheological parameters such as the shear stress σ , and the first and second normal stress differences N_1 and N_2 in the $t \rightarrow \infty$ limit:

$$\sigma(\infty, \dot{\gamma}) = \frac{G_o}{2\tau_R \dot{\gamma}} (\sqrt{1 + 4\tau_R^2 \dot{\gamma}^2} - 1) \quad (10)$$

$$N_1(\infty, \dot{\gamma}) = 2G_o \frac{1 - \Lambda^2}{\Lambda} \quad (11)$$

$$N_2(\infty, \dot{\gamma}) = G_o(\Lambda - 1) \quad (12)$$

where $\Lambda^2 = \frac{\sqrt{1+4\tau_R^2\dot{\gamma}^2}-1}{2\tau_R^2\dot{\gamma}^2}$. In the Giesekus model, the shear viscosity $\eta(\dot{\gamma})$ is given by

$$\eta(\dot{\gamma}) = \frac{\eta_o}{2\tau_R^2\dot{\gamma}^2}(\sqrt{1+4\tau_R^2\dot{\gamma}^2}-1) \quad (13)$$

1.1.3 Cox-Merz rule

The Cox-Merz rule is a semi-empirical rule which relates the complex viscosity $\eta^*(\omega)$ with the shear viscosity $\eta(\dot{\gamma})$ in the following way :

$$\eta(\dot{\gamma}) = |\eta^*(\omega)|, \quad \omega = \dot{\gamma} \quad (14)$$

The shear viscosity $\eta(\dot{\gamma})$ is predicted by the Giesekus model and is given by Eqn. 13. The dynamic viscosity may be calculated from the viscoelastic moduli using Eqn. 5 and may be fitted to Eqn. 6. For the CTAB/ NaSal (60mM/ 350mM) system forming giant wormlike micelles, a relatively good agreement to the Cox-Merz rule is observed [9].

1.1.4 Connected micelles

For suitably high concentrations of the added electrolyte, many of the measured rheological properties of entangled micellar solutions are found to deviate considerably from the predictions of the reptation-reaction theory [2]. Unusually high fluidity has been observed in aqueous micellar solutions of the system cetylpyridinium chlorate (CPClO₃) / sodium chlorate (NaClO₃) [13]. For the system hexadecyltrimethylammonium bromide (CTAB)/ potassium bromide (KBr)/ water, Khatory *et al.* have observed anomalous scaling of the zero shear viscosity η_o and the high frequency plateau modulus G_o with surfactant concentration [14]. The zero-shear viscosity η_o of cetyltrimethylammonium chloride (CTAC) and sodium salicylate (NaSal) shows a peak at $\frac{[NaSal]}{[CTAC]} \sim 0.6$ [15]. The increase and decrease of η_o obey power-law scaling relations with CTAC concentration, characterized by exponents 1.1 and -2.1 respectively. A peak in the zero-shear viscosity has also been observed in aqueous solutions of CPyCl/NaSal at $\frac{[NaSal]}{[CPyCl]} \sim 1$ [16]. These results cannot be explained in terms of the theory for entangled micelles [5], but can be understood by considering intermicellar branching at high salt concentrations. These connections between micelles characterize a new relaxation process which involves the sliding of connections along the micelles [17, 18].

The general features of stress relaxation seen in linear micelles are preserved in the case of branched micelles if one replaces the average length \bar{L} by a new length \bar{L}_c , where $\bar{L}_c = \frac{n_2}{n_1+2n_3}l_p$ [14, 18]. In the expression for \bar{L}_c , l_p is the persistence length, n_1 is the concentration of the end caps, n_2 is the number density of the persistence lengths and n_3 is the number density of 3-fold network junctions. This model gives rise to a relaxation process that is faster than the predictions of the theory for reptation and reversible scission [5], and explains the anomalously high fluidity seen in some systems of wormlike micelles at high salt or surfactant concentrations [14, 15].

2 Sample preparation and apparatus used

Samples of CTAT/ NaCl/ water were prepared by weighing out the requisite quantity of CTAT in a microbalance and dissolving it in brine (solution of NaCl in deionized and distilled water) prepared at the following concentrations: 0 mM, 0.5mM, 1mM, 2mM, 5mM, 10mM, 20mM, 40mM, 60mM, 80mM, 90mM, 100mM and 120mM. The concentration of CTAT in the brine solution was kept constant at 42mM (1.9 wt.%). The samples were kept in an incubator at 30°C for a week and shaken frequently to ensure homogenization. All the experiments reported below were conducted at a fixed temperature of 25°C. The oscillatory and flow measurements were performed in an AR 1000N stress controlled rheometer (T. A. Instruments, U. K.), using a cone-and-plate geometry of radius 4 cm and angle 1°59'. Sponges were used as solvent traps to prevent evaporation of the solvent (water) during the experiment.

3 Experimental results

In this section, we first describe the linear rheology results (section 3.1), followed by the nonlinear rheology results (section 3.2) and attempt to correlate the results obtained from the two, with an aim to understanding the flow behavior of CTAT in the presence of salt (section 4).

3.1 Linear Rheology

Fig. 1 shows the frequency response ($G'(\omega)$ and $G''(\omega)$ vs. ω) measurements for CTAT/ NaCl/ water for a few typical salt concentrations ($c_{NaCl} =$ (a) 0mM, (b) 20mM, (c) 60mM and (d) 100mM) over three decades of angular frequencies, and the corresponding fits to the real and imaginary parts of the Cole-Davidson form given by Eqn. 9 (shown by solid lines in each plot).

The fits to the Cole-Davidson form of the frequency response data in the presence of 20 - 120mM NaCl yield $\alpha \sim 0.80 - 0.90$, in comparison to the unscreened micellar phase (0 mM NaCl) where $\alpha \sim 0.15$. For the NaCl concentrations of 0.5mM, 1mM, 2mM, 5mM and 10mM, the values of α are found to increase with increasing molarity of the brine solution. Fig. 2 shows the values of α obtained from the Cole-Davidson fit as a function of salt concentration, which indicates a gradual crossover from non-exponential to single-exponential stress relaxation on the addition of NaCl to CTAT solutions. Similar observations by Rehage *et al.* [1, 16] on adding NaSal to CPyCl solutions have been explained in terms of a crossover from diffusion-controlled to kinetically-controlled stress relaxation processes. The fits shown in Fig. 1 also give us estimates of the high frequency plateau modulus G_o and the terminal relaxation time τ_R . The values of τ_R have also been calculated from the crossover frequency ω_{co} using the relation $\tau_R = \frac{1}{\omega_{co}}$ (Fig. 7(a)). The data acquired in the presence of 20 - 120mM NaCl can also be fitted satisfactorily to the Maxwell model [2] as is seen from the semicircular nature of the Cole-Cole plots ($\frac{G'(\omega)}{G_o}$ versus $\frac{G''(\omega)}{G_o}$ plotted in Fig. 3). G_o is the value of the high frequency plateau modulus obtained from fits to the Cole-Davidson model.

The Cole-Cole plots for the CTAT samples with low salt content (≤ 5 mM) are found to deviate considerably from the semicircular behavior characteristic of a Maxwellian fluid. We note that these deviations at high frequencies ($\omega \geq \omega_b$) and the subsequent upturn ($\omega \geq \omega_e$) in the Cole-Cole plots are due to the reversible breaking of the wormlike chains at a characteristic time τ_{break} and the contribution of the localized dynamics between entanglements (the Rouse modes), respectively [19]. The absence of a well-defined plateau in the elastic modulus $G'(\omega)$ of the samples with low salt content at high angular frequencies ω , is possibly due to long breaking times or the occurrence of Rouse modes at relatively low frequencies.

Fig. 4 shows the plots of the complex viscosities $\eta^*(\omega)$ vs. ω measured for the

samples with c_{NaCl} equal to (a) 0mM, (b) 20mM, (c) 60mM and (d) 100mM, *vs.* the angular frequencies ω , and the corresponding fits to the model for giant wormlike micelles given in Eqn. 6 [9]. The fits, shown by solid lines, are found to be poor for the unscreened case, but agree very well with the experimental data for the samples with high concentrations of added salt ($c_{NaCl} \geq 20\text{mM}$). The values of η_o obtained from these fits are shown in Fig. 7(c) by solid triangles.

3.2 Nonlinear rheology

Nonlinear rheology measurements have been used to estimate the zero-shear viscosity η_o and the relaxation time τ_R from the flow curves. Here the shear stress σ and the viscosity η are measured simultaneously as a function of the shear rate $\dot{\gamma}$. Fig. 5 shows the fits (shown by solid lines) to the Giesekus model (Eqn. 13) of the shear viscosities $\eta(\dot{\gamma})$ (indicated by circles) *vs.* shear rates $\dot{\gamma}$ for the samples with salt content (a) 0mM, (b) 20mM, (c) 60mM and (d) 100mM respectively. For high salt concentrations, the fits to the Giesekus model are found to deviate considerably from the experimental data at high values of $\dot{\gamma}$. The values of η_o and τ_R obtained from these fits are compared to those obtained from the fits to $\eta^*(\omega)$ (Table 1). The values thus calculated from the linear and nonlinear rheology measurements deviate considerably from each other at low salt concentrations but show some agreement at $c_{NaCl} \geq 20\text{mM}$.

4 Discussions

In this section, we will attempt to quantify and understand the changes in the viscoelastic parameters of the CTAT/ NaCl/ water samples due to the increased screening of intermicellar interactions as a result of the addition of salt.

4.1 Applicability of the Cox-Merz rule

As discussed in section 1.1.3, viscoelastic gels usually follow the empirical Cox-Merz rule [9]. To see this in the present case, we have plotted in Fig. 6 the normalized viscosities $\frac{\eta^*(\omega)}{\eta_o}$ and $\frac{\eta(\dot{\gamma})}{\eta_o}$ versus angular frequency ω and shear

Table 1: The parameters τ_R and η_o , obtained from the fits of $\eta^*(\omega)$ vs. ω to Eqn. 6 (denoted by *DV*) and from the fits of $\eta(\dot{\gamma})$ vs. $\dot{\gamma}$ to the Giesekus model (Eqn. 13, denoted by *GM*) are tabulated below :

NaCl (mM)	τ_R s(DV)	τ_R s (GM)	η_o Pa-s (DV)	η_o Pa-s (GM)
0	8.78	12.88	42.42	36.69
0.5	13.93	21.03	49.62	36.72
1	15.16	24.5	62.13	51.02
2	15.77	22.35	80.27	70.43
5	36.69	31.61	42.42	39.05
10	6.00	7.2	45.52	46.08
20	3.53	3.44	38.7	44.35
40	2.30	1.77	32.49	22.21
60	1.79	1.46	27.98	29.63
80	1.51	1.06	17.09	15.24
90	1.30	0.98	11.14	11.72
100	1.21	0.58	9.50	6.74
120	1.08	0.50	6.56	6.03

rate $\dot{\gamma}$ respectively for c_{NaCl} equal to (a) 0mM, (b) 20mM, (c) 60mM and (d) 100mM. The curves show an excellent superposition at $c_{NaCl}=60\text{mM}$ ($\frac{[NaCl]}{[CTAT]}=1.42$) over the entire range of ω and $\dot{\gamma}$. We notice significant deviations in the values of $\frac{\eta^*(\omega)}{\eta_o}$ and $\frac{\eta(\dot{\gamma})}{\eta_o}$ at high ω and $\dot{\gamma}$ at very low and very high salt concentrations.

4.2 Existence of three regimes of contrasting flow behaviors

Fig. 7(a) shows the relaxation time τ_R , obtained using the relation $\tau_R \sim \omega_{co}^{-1}$, *vs.* c_{NaCl} . On increasing c_{NaCl} , τ_R shows an initial increase, followed by a strong decrease. The dependence of τ_R on c_{NaCl} in these regimes may be fitted to the relation $\tau_R \sim c_{NaCl}^\beta$ (shown by solid lines in Fig. 7(a)). The values of β is +0.11 for $c_{NaCl} \leq 2\text{mM}$ (regime I, $\frac{[NaCl]}{[CTAT]} \leq 0.05$), and changes to -0.65 thereafter.

Fig. 7(b) shows the plots of the high frequency plateau modulus G_o obtained in the following ways: the values obtained from the Cole-Davidson fits (solid circles), and the values of $G'(\omega)$ at a high frequency $\omega = 29 \text{ rads}^{-1}$ (solid triangles). The two sets of values of G_o deviate considerably at $c_{NaCl} \leq 2\text{mM}$ (regime I), but agree very well at higher salt concentrations ($c_{NaCl} \geq 5\text{mM}$). At $5\text{mM} \leq c_{NaCl} \leq 60\text{mM}$, G_o increases with salt concentration, followed by a decrease at $c_{NaCl} \geq 60\text{mM}$. These two regimes, characterized by different slopes (shown in Fig. 7(b) and marked as regimes II and III), have been fitted to $G_o \sim c_{NaCl}^{\beta'}$, where $\beta'=0.31$ in regime II and -1.38 in regime III.

The same three regimes can be very clearly distinguished in Fig. 7(c), where η_o is plotted *vs.* c_{NaCl} . The values of η_o are obtained from the fits of η^* (solid triangles) and $\eta(\dot{\gamma})$ (solid circles) discussed above. η_o shows an initial increase in regime I, followed by a weak decrease in regime II and subsequently, a much stronger decrease in regime III. In all the three regimes, η_o has been fitted to the power law $\eta_o \sim c_{NaCl}^{\beta''}$, where β'' is equal to 0.35 in regime I (fit shown by dashed line), -0.29 in regime II (fit shown by solid line) and -2.04 in regime III (fit shown by dashed line). The weak increase in η_o at low c_{NaCl} may be explained in terms of micellar growth as a result of enhanced screening of intermicellar interaction on the addition of NaCl. The subsequent decrease in η_o at high c_{NaCl} may be explained in terms of intermicellar connections [1, 14, 15]. We would like to note here that fluorescence recovery after fringe

pattern photobleaching (FRAPP) experiments have also shown an increase in the diffusion coefficients (*i.e.* a decrease in the effective viscosity) of aqueous, semi-dilute solutions of CTAT micelles in the presence of 0.1 M and 1 M NaCl with increasing CTAT concentrations [20]. This effect increases with the increase in the salt concentration and has been explained in terms of connected micelles. These intermicellar connections serve as sliding contacts, aiding the faster reptation of the micelles, and hence decreasing the viscosity of the system [18]. An interesting feature of our data is the existence of two distinct regimes (regimes II and III in Fig. 7(c)) where η_o shows a decrease with c_{NaCl} . In contrast to previous experiments with gemini surfactants [3], there is a regime of weak decrease of η_o (regime II) followed by a much stronger decrease on increasing c_{NaCl} (regime III). At the cross-over between regimes II and III ($c_{NaCl} = 60\text{mM}$), the change in the slope of η_o (Fig. 7(c)) is accompanied by a change in the sign of the slope of G_o , as shown in Fig. 7(b). In regime II, G_o shows an anomalous increase with c_{NaCl} .

The addition of salt is known to encourage micellar growth [2]. However, as the CTAT concentration is fixed and lies in the semi-dilute regime, we do not expect ξ , the correlation length of concentration fluctuations to change appreciably. For flexible micelles, the correlation length ξ is related to G_o as $G_o \sim \frac{k_B T}{\xi^3}$ [2]. The plateau modulus G_o may be written as $G_o \sim \frac{ck_B T}{l_e}$, where c is the macromolecule concentration and l_e is the entanglement length [7]. l_e scales with the persistence length l_p and the correlation length ξ as $l_e \sim \frac{\xi^{5/3}}{l_p^{2/3}}$.

An increase in G_o , therefore, implies a decrease in entanglement length l_e and an increase in the persistence length l_p . An increase in l_p is indicative of an increase in the surface charge of the micelles. Such an increase in the surface charge could occur due to the unbinding of the tosylate counterions from CTA^+ on the addition of NaCl [21]. Low-frequency conductivity measurements have confirmed the phenomenon of counterion unbinding in the liquid crystalline phase of cesium perfluoro-octanol (CsPFO)/ PFO/ water on the addition of alcohol [22]. However, at $c_{NaCl} \geq 60\text{mM}$ (regime III), the micelles are again screened completely, as indicated by the decrease in G_o and η_o in this regime. We would like to note here that the decrease in viscosity of the system CTAC/NaSal with increasing concentrations of CTAC follows the relation $\eta_o \sim c_{NaCl}^{\beta''}$, where $\beta'' = -2.1$ [15], very close to the value $\beta'' = -2.04$ obtained by us in regime III.

4.3 Superposition of the linear and nonlinear rheology data for CTAT/ NaCl/ water

In this section, we discuss the superposition of the frequency response and flow curves of the CTAT/ NaCl/ water samples. In Figs. 8 and 9, we have plotted master curves by normalizing the viscoelastic parameters by suitable quantities. The elastic and viscous moduli are normalized by $\frac{\eta_0}{\tau_R}$, the dynamic viscosity η^* by $G_0\tau_R$, the shear stress σ by G_0 and the shear rate $\dot{\gamma}$ by τ_R^{-1} , respectively. Similar master curves for the linear rheology data of CTAT have been observed by Soltero *et al.* [23] on increasing the concentration of CTAT. In Fig. 8, (a) and (b) correspond to the plots of the normalized $G''(\omega)$ and $G'(\omega)$ data respectively, while (c) shows the plots of the normalized dynamic viscosity $\eta^*(\omega)$. The curves for the normalized $G''(\omega)$ at 0mM NaCl are found to deviate considerably from the master curve on which the data corresponding to $c_{NaCl} \geq 20$ mM lie, which is indicative of a large difference in the viscous flow properties of CTAT in the screened and unscreened limits.

It is also possible to superpose the normalized stress $\frac{\sigma}{G_0}$ *vs.* the normalized shear rate $\dot{\gamma}\tau_R$ plots of the CTAT/ NaCl/ water samples. All the flow curves are found to superpose very well in the regime of low $\dot{\gamma}\tau_R$ (Newtonian regime, characterized by unit slope of σ *vs.* $\dot{\gamma}$ on a log-log plot), but show deviations at higher values of $\dot{\gamma}\tau_R$ (Fig. 9). The normalized shear stress is found to level off to a plateau at $\dot{\gamma}\tau_R \sim 1$, with the slope of the plateau increasing monotonically with increase in salt concentrations. Berret *et al.* [24] have observed perfect superposition for CPyCl /NaSal/ water samples in the Newtonian regime of the flow curve, while the slope of the normalized stress in the plateau (nonlinear) regime increases on increasing the sample temperature. Interestingly, the branching of the micelles that we observe at $c_{NaCl} \geq 20$ mM does not have any significant effect on the master phase diagrams obtained from the linear rheology experiments (Fig. 8). The normalized flow curves of CTAT/ NaCl/ water, however, show a significant change in the slope of the 'plateau' region on increasing c_{NaCl} , which points to a change in the non-linear flow behavior of the aqueous CTAT/ NaCl samples on the addition of salt.

5 Conclusions

In this paper, we have discussed the modifications of the viscoelastic properties of CTAT (concentration of CTAT is kept fixed at 42mM) as a result of the addition of the salt. We find that the data may be divided into three distinct regimes, where η_o and G_o can be fitted to different power-laws. The decrease of η_o at high salt concentration has been explained in terms of intermicellar branching [18]. The anomalous increase of G_o on increasing salt concentration has been explained in terms of tosylate unbinding from the CTA⁺ on the addition of salt. It will be interesting to understand the precise mechanism of this counterion unbinding phenomenon. Significantly, at $c_{NaCl}=60\text{mM}$, the persistence length of the micelles is maximum, which indicates the presence of highly charged micelles at these concentrations. Interestingly, the scaling of τ_R on c_{NaCl} does not change from regime II to regime III. As shown in Fig. 6, the superposition between $\eta^*(\omega)$ and $\eta(\dot{\gamma})$ is very good at $c_{NaCl}=60\text{mM}$. It is also worth noting that the branching of the micelles does not appreciably alter the scaling of the linear rheology parameters (plots of normalized $G'(\omega)$, $G''(\omega)$ and $\eta^*(\omega)$ for $c_{NaCl} \geq 20 \text{ mM}$, shown in Fig. 8). In contrast, when the flow curves are superposed to lie on a single master curve, we find that the slope of the plateau increases on increasing c_{NaCl} , indicating a modification of the shear banding properties of the samples in the presence of intermicellar connections. Significant changes in the nonlinear flow behavior of CTAB/ NaSal/ water have been observed from small angle light scattering experiments on increasing salicylate counterions [25].

In the light of the present work, it will be worthwhile to study more exhaustively the linear and nonlinear rheology of cylindrical micelles as a function of the surface charge, with and without multiconnected junctions. Anomalous flow properties of surfactant systems like CPyCl/ NaSal/ water have been previously observed at about equimolar proportions of CPyCl and NaSal [1, 16]. Till date, there have been several studies on the effect of the chemical formula and lipophilicity of the counterions on the growth of a micelle [26, 27]. It will be extremely interesting to undertake a detailed study of the effects of the chemical nature of the counterion on its unbinding from a micelle.

6 Acknowledgements

The authors would like to thank Prof. M. Cates for useful discussions. They would like to thank Profs. S. Ramaswamy, P. R. Nott and V. Kumaran for the use of the rheometer.

References

- [1] Rehage, H.; Hoffmann, H. *Mol. Phys.* **1991**, *74*, 933.
- [2] Cates, M. E.; Candau, S.J. *J. Phys. Condens. Matter* **1990**, *2*, 5869.
- [3] Kern, F.; Lequeux, F.; Zana R.; Candau, S. J. *Langmuir* **1994**, *10*, 1714.
- [4] Kern, F.; Zana, R.; Candau, S. J. *Langmuir* **1991**, *7*, 1344.
- [5] Cates, M. E. *Macromol.* **1987**, *20*, 2289; Cates, M. E. *J. Phys. Chem.* **1990**, *94*, 371.
- [6] Mackintosh, F. C.; Safran S. A.; Pincus, P. A. *Europhys. Lett.* **1990**, *12*, 697.
- [7] deGennes, P. G. In *Scaling Concepts in Polymer Physics*, Cornell University Press, Ithaca, New York, 1979.
- [8] Doi, M.; Edwards, S. F. In *The Theory of Polymer Dynamics*, Oxford Clarendon, 1986.
- [9] Fischer, P.; Rehage, H. *Rheol. Acta* **1997**, *36*, 13.
- [10] Menon, N.; Nagel, S. R.; Venerus, D. C. *Phys. Rev. Lett.* **1994**, *73*, 963.
- [11] Candau, S. J.; Hirsch, E.; Zana, R.; Delsanti, M. *Langmuir* **1990**, *5*, 1525.
- [12] Giesekus, H. *J. Non-Newt. Fluid Mech.* **1982**, *11*, 69.
- [13] Appell, J. *et al.*, *J. Phys. II France* **1992** *2*, 1045.

- [14] Khatory, A.; Lequeux, F.; Kern, F.; Candau, S. J. *Langmuir* **1993**, *9*, 1456.
- [15] Aït Ali, A.; Makhloufi, R. *Phys. Rev. E* **1997**, *56*, 4474.
- [16] Rehage, H.; Hoffmann, H. *J. Phys. Chem.* **1998**, *92*, 4716.
- [17] Drye, T. J.; Cates, M. E. *J. Chem. Phys.* **1992**, *96*, 1367.
- [18] Lequeux, F. *Europhys. Lett* **1992**, *19*, 675.
- [19] Granek, R.; Cates, M. E. *J. Phys. Chem.* **1992**, *96*, 4758.
- [20] Narayanan, J.; Manohar, C.; Langevin, D.; Urbach, W. *Langmuir* **1997**, *13*, 398.
- [21] Cates, M. E. private communication.
- [22] Li, Z.; Rosenblatt, C. *J. Chem. Phys.* **1998**, *89*, 5033.
- [23] Soltero, J. F. A.; Puig, J. E.; Manero, O. *Langmuir* **1996**, *12*, 2654.
- [24] Berret, J. F.; Porte, G.; Decruppe, J. P. *Phys. Rev. E* **1997**, *55*, 1668.
- [25] Kadoma, I. A.; van Egmond, J. W. *Langmuir* **1997**, *13*, 4551.
- [26] Magid, L. J. *et al.*, *J. Phys. Chem. B* **1997**, *101*, 7919.
- [27] Oda, R. *et al.*. *Langmuir* **1988**, *14*, 4364.

7 Figure Captions

Figure 1: The frequency response curves ($G'(\omega)$ denoted by circles and $G''(\omega)$ denoted by triangles versus the angular frequency ω) of aqueous solutions of 42mM CTAT + NaCl and their corresponding fits to the Cole-Davidson model (shown by solid lines). The CTAT concentration is maintained constant at 42mM while the NaCl concentrations corresponding to the graphs are (a) 0mM, (b) 20mM, (c) 60mM, (d) 100mM.

Figure 2: Plot of the values of α obtained from the fits to the Cole-Davidson model *vs.* the salt concentration c_{NaCl} . The concentration of CTAT is fixed at 42mM.

Figure 3: Normalized Cole-cole plots obtained by plotting $\frac{G'(\omega)}{G'_o}$ *vs.* $\frac{G''(\omega)}{G''_o}$ for CTAT (42mM)/ NaCl/ water. The different symbols correspond to the following NaCl concentrations: (a) squares for 0mM, (b) plus-centred squares for 0.5mM, (c) plus-centred circles for 1mM, (d) dash-centred squares for 2mM, (e) \times -centred circles for 5mM, (f) circles for 20mM, (g) up-triangles for 40mM, (h) down-triangles for 60mM, (i) plus signs for 80mM, (j) \times signs for 90mM, (k) \star signs for 100mM and (l) - for 120mM.

Figure 4: The dynamic viscosity $\eta^*(\omega)$ versus ω for CTAT (42mM)/ NaCl/ water samples. The solid lines show the fits to Eqn. 6. The NaCl concentrations corresponding to each plot is as follows: (a) 0mM, (b) 20mM, (c) 60mM, (d) 100mM.

Figure 5: The viscosity $\eta(\dot{\gamma})$ versus $\dot{\gamma}$ for 42mM CTAT + NaCl samples. The NaCl concentrations corresponding to each plot is as follows: (a) 0mM, (b) 20mM, (c) 60mM, (d) 100mM. The solid lines show the fits to the Giesekus model.

Figure 6: The normalized shear viscosity $\frac{\eta(\dot{\gamma})}{\eta_o}$ (circles) and normalized dynamic viscosity $\frac{\eta^*(\omega)}{\eta_o}$ (triangles) plots versus $\dot{\gamma}$ and ω for CTAT (42mM)/ NaCl/ water samples. The NaCl concentrations corresponding to each plot is as follows: (a) 0mM, (b) 20mM, (c) 60mM, (d) 100mM. The solid lines

show the fits to the Giesekus model.

Figure 7: The values of τ_R , obtained from the crossover frequency ω_{co} of G' and G'' , have been plotted in (a) *vs.* c_{NaCl} . In (b) we have plotted the values of G_o obtained from the fits to the Cole-Davidson model (indicated by filled circles) and from the values of G' at $\omega = 29 \text{ rads}^{-1}$ (filled triangles). (c) shows the plots of the zero-shear viscosities η_o with increasing c_{NaCl} , obtained from the fits to the dynamic viscosity η^* (solid triangles) and the fits to the Giesekus model of the shear viscosity η (solid circles). The solid and dashed lines are the fits to $A \sim c_{NaCl}^\beta$, $A = \tau_R, G_o$ and η_o . The values of β in each regime are noted on the graphs.

Figure 8: (a) and (b) show the values of $G''(\omega)$ and $G'(\omega)$, both scaled by $\frac{\eta_o}{\tau_R}$ *vs.* $\omega\tau_R$. Apart from the measurements with 0mM NaCl (depicted by squares), all other curves lie on a master curve. (c) shows the scaled dynamic viscosity $\frac{\eta^*(\omega)}{G_o\tau_R}$ *vs.* $\omega\tau_R$. In the diagrams, circles correspond to 20mM NaCl, up-triangles for 40mM, down-triangles for 60mM, plus signs for 80mM, cross signs for 90mM, stars for 100mM and bars for 120mM.

Figure 9: The normalized flow curves of CTAT (42mM)/ NaCl/ water, where σ and $\dot{\gamma}$ are scaled as $\sigma \rightarrow \frac{\sigma}{G_o}$ and $\dot{\gamma} \rightarrow \dot{\gamma}\tau_R$. In the diagrams, squares stand for 0mM NaCl while the keys for the other symbols are the same as in Fig. 8.

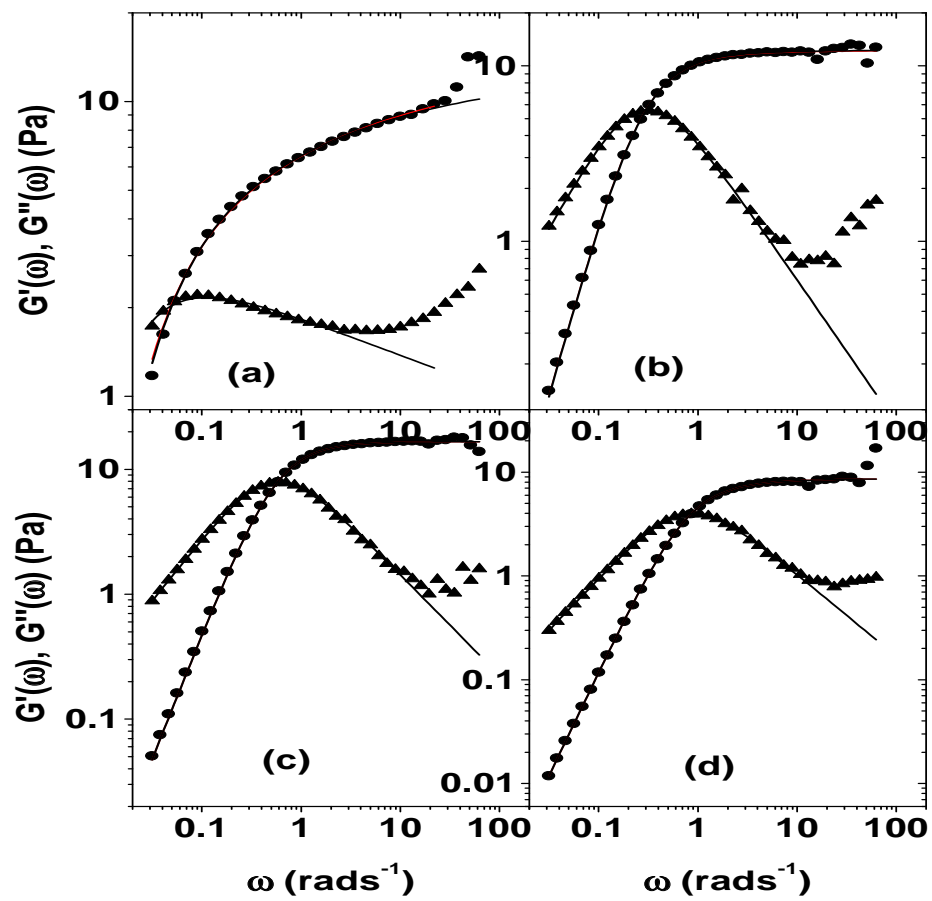


Figure 1

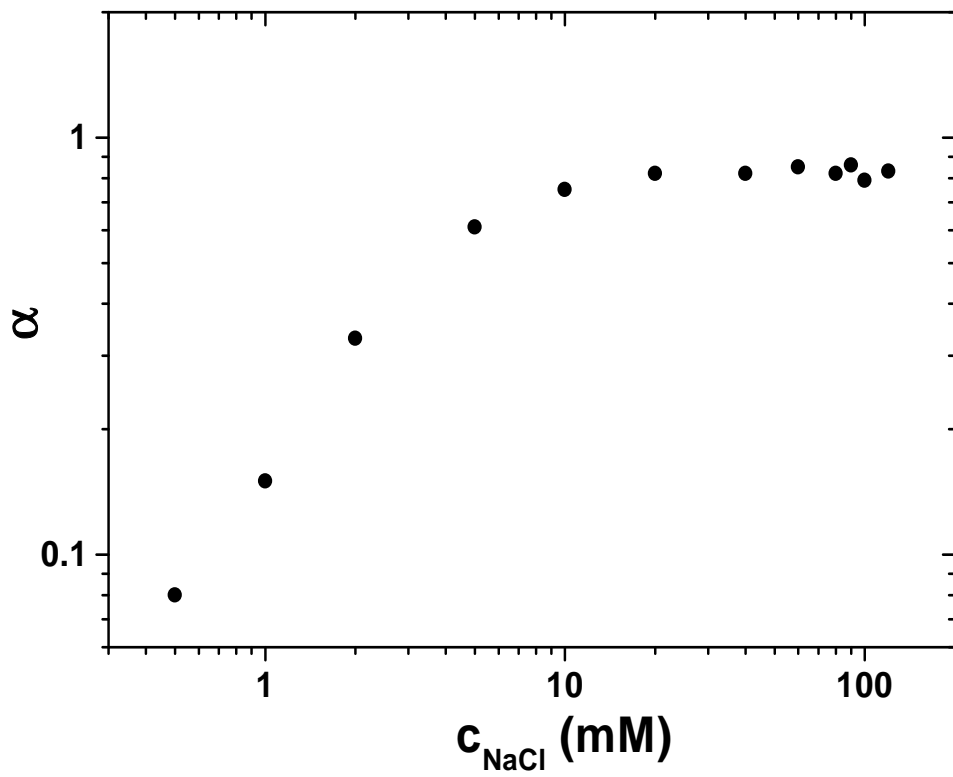


Figure 2

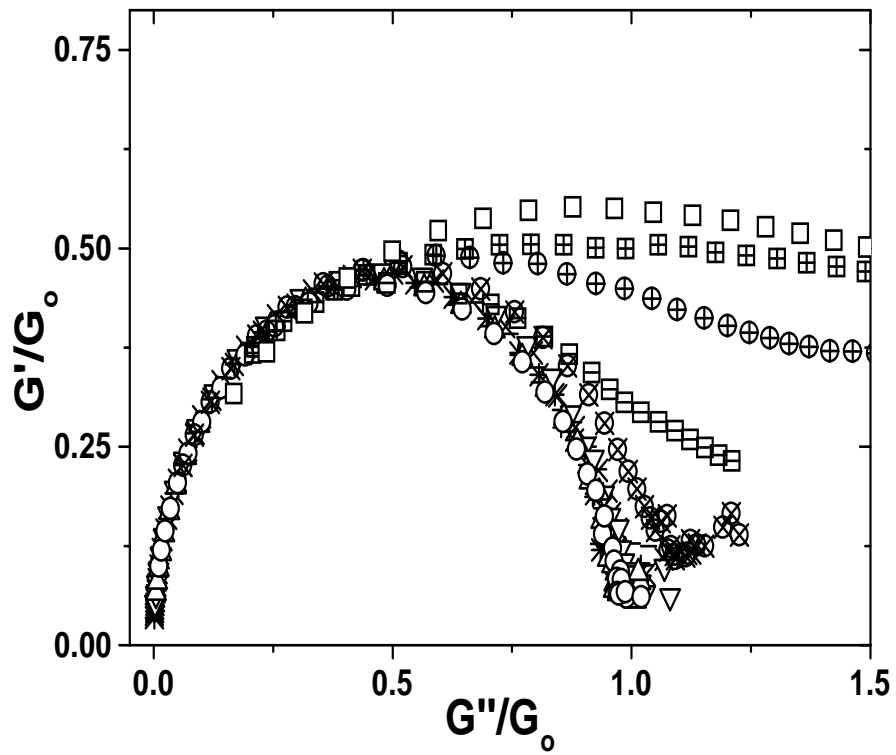


Figure 3

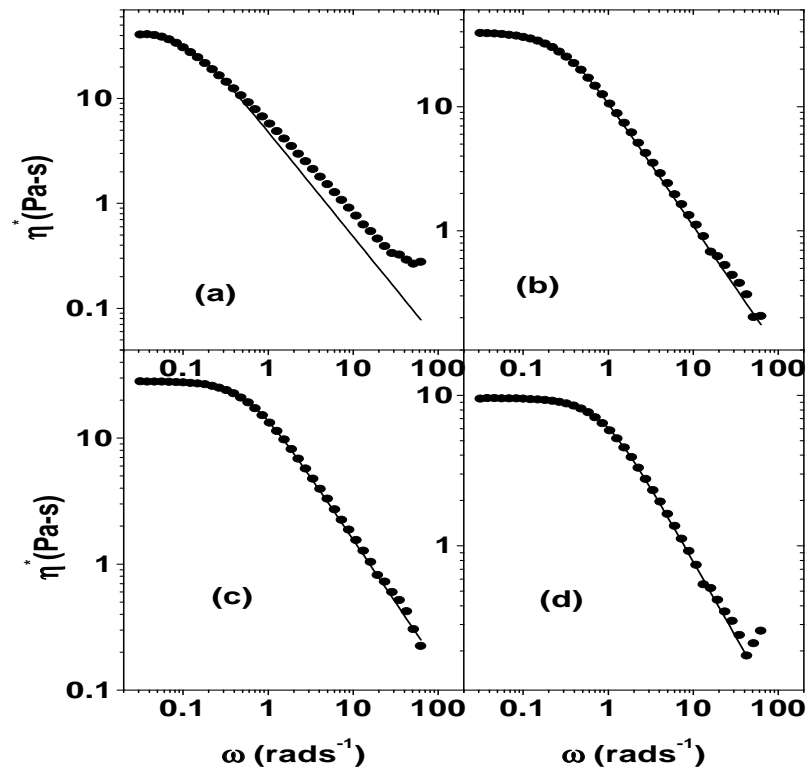


Figure 4

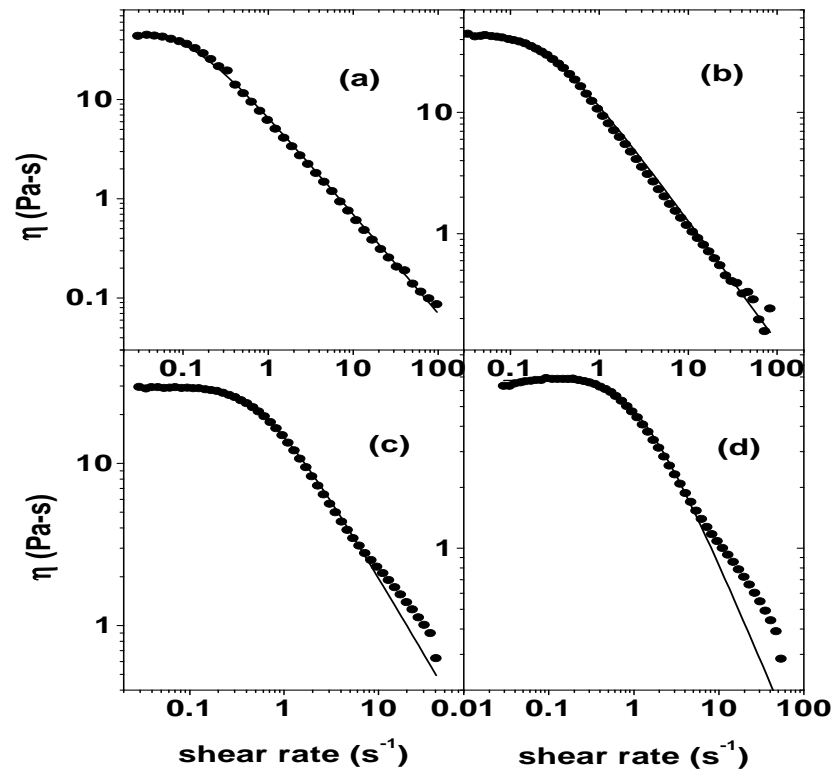


Figure 5

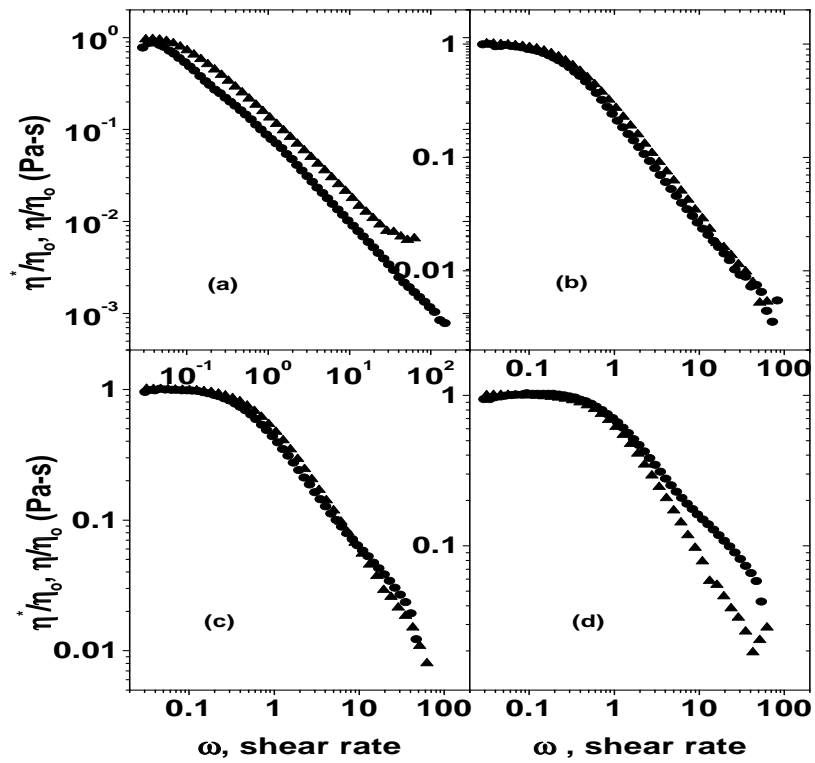


Figure 6

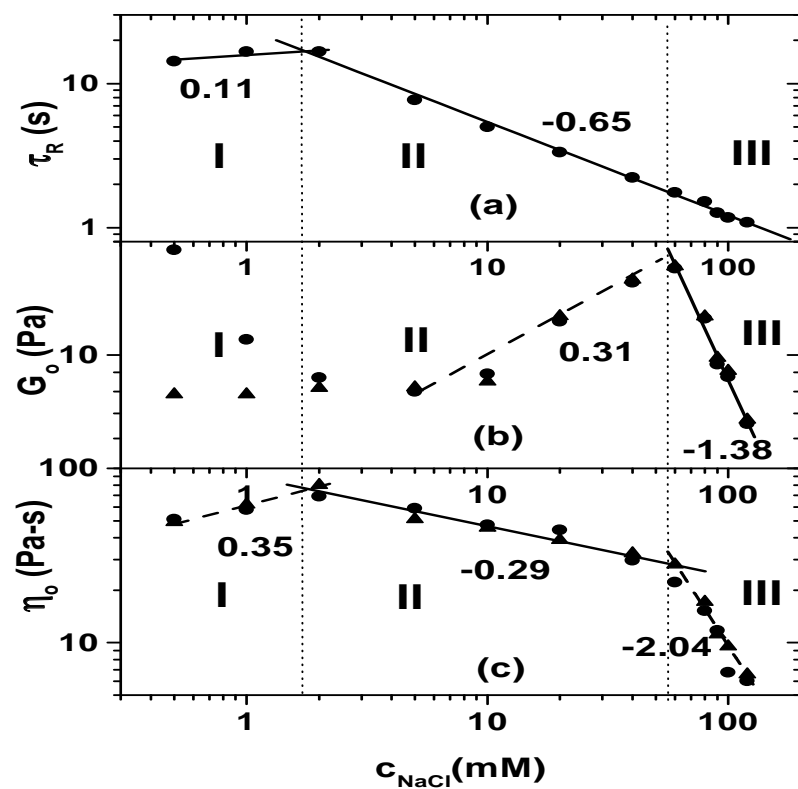


Figure 7

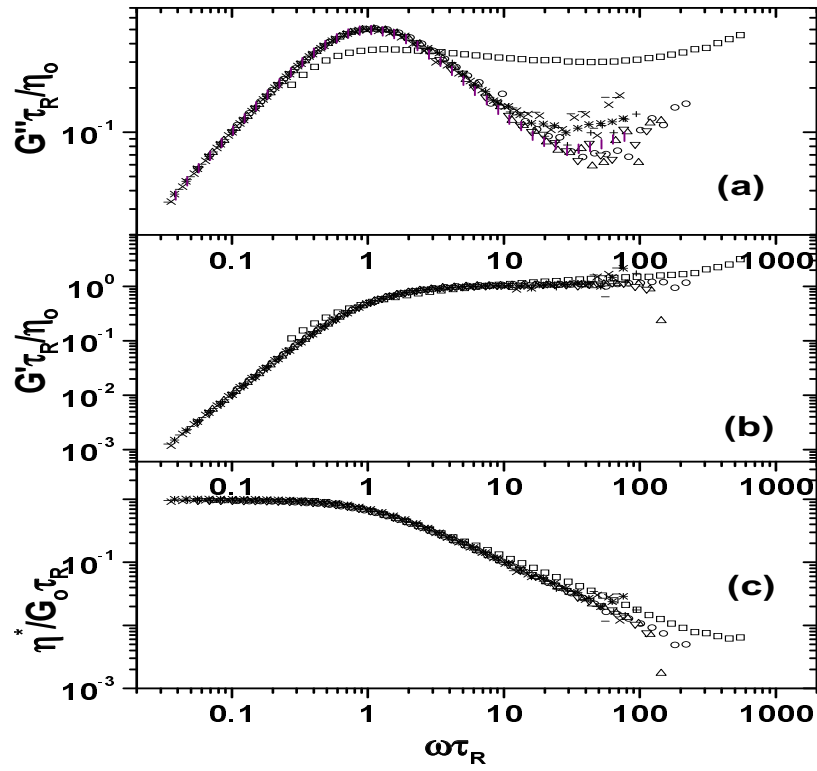


Figure 8

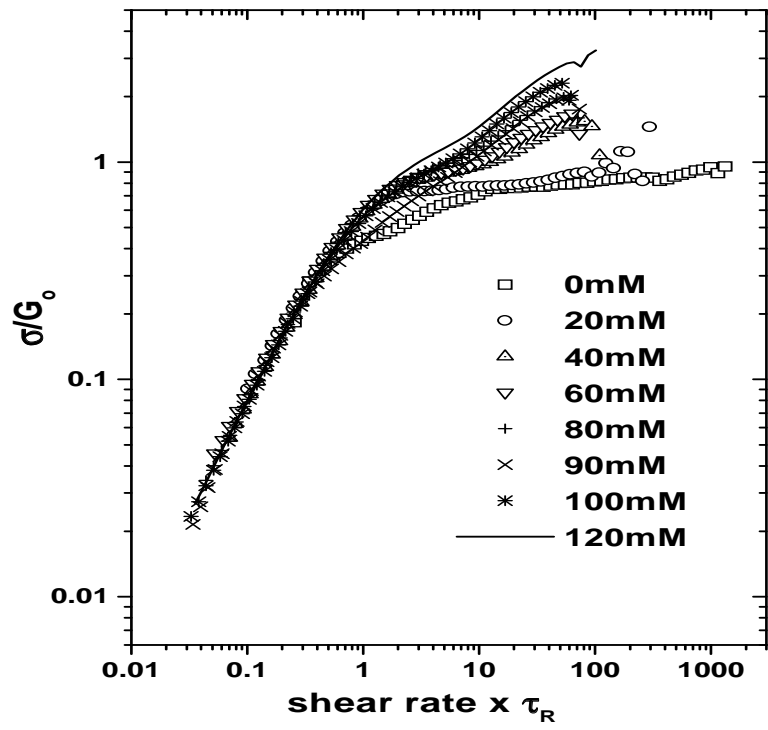


Figure 9